# Simulation Analysis of Pipeline Detection Robot Motion State

Leiyu Gong [1, a], Shengli Zhou [2, b], Cheli Ren [3, c], and Weikai Zhao [1, d]

[1]School of Automation Science and Electrical Engineering, Beihang University, Beijing, 100191, China;

[2] Project Department of SSSG-7 Bid of Shenzhen-Shantou Railway, China Railway 14th Bureau Group Grand Shield Engineering Co, Shenzhen, 528100, China.

[3] Zhejiang Easun Pneumatic Science & Technology Co., Ltd., Ningbo, 315300, China.

[a] 1163245987@qq.com, [b] 1094922771@qq.com, [c] rencheli@china-easun.com,

[d] zwk@buaa.edu.cn

**Abstract.** Pipeline transportation has the advantages of safety, reliability and low energy consumption in transporting natural gas, and is an important transportation route for transporting natural gas. Due to the characteristics of natural gas pipelines with large internal pressure fluctuations, plenty of pipeline bending sections and complex pipeline deformation characteristics, pipeline detection robots are required to have higher detection capabilities, and the study of the motion state of natural gas pipeline detection robots in pipeline detection is of practical significance. This paper adopts the CFD numerical simulation method and establishes the model of DN800 pipeline deformation detection robot. Next, by simulating the natural gas pipeline detection robot under different media and different pipeline types respectively, the motion state of the detection robot is analyzed under different conditions. The simulation results verify the reliability of the detection robot working inside the pipeline, which can fully guarantee the safe transportation of natural gas pipeline.

**Keywords:** natural gas pipeline; pipeline detection robot; CFD; motion state.

## 1. Introduction

Natural gas is widely used in everyday life and industrial activities because of its high calorific value per unit, low price, low environmental impact and reliable supply sources compared to oil and coal [1]. The main method of transporting natural gas is long pipeline transportation, which is the optimal solution for transporting natural gas and oil because of its large volume, low volume of transport work, small footprint, low energy consumption, and high safety and reliability of continuous transport. Due to the large geographical span of transportation, various geological hazards are prone to cause damage to pipelines and affect the normal transportation of natural gas [2]. In order to be able to properly diagnose the fault deformation of pipelines, guarantee the normal driving of pipelines and avoid safety accidents, pipeline inspection robots have been invented at home and abroad.

At home and abroad, the research of pipeline inspection robots has been relatively mature, and a variety of pipeline robots with different operating structures have been developed, such as wheeled, crawler, walking and so on [3,4,5,6,7,8]. Compared with other robots, the fluid-driven pipeline inspection robot is driven by the fluid pressure difference between the front and rear, overcoming the friction between the two walls of the pipeline and advancing forward, without the need for additional motors or external environment to provide power to complete the pipeline inspection task at a certain speed, the speed can be different depending on the actual robot ends of the pressure difference, the greater the difference between the upstream and downstream hydraulic pressure in the pipeline, the faster the pipeline inspection robot will move. The greater the difference in hydraulic pressure between upstream and downstream in the pipe, the faster the pipeline inspection robot will move [9,10,11]. For this reason, this paper uses CFD to analyze the flow field around the robot when it is filled with different fluid media in different pipeline types to provide a reference aspect for controlling the robot's operating speed in the pipeline.

# 2. Model, Assumptions and Equations

## 2.1 Geometric Model Simplification.

As the actual model is more precise, the pipeline inspection robot cannot be restored with accuracy in model building. Reasonable assumptions are used to simplify the model by removing the parts that have no effect on the flow field analysis, and the final model obtained is shown in the Fig. 1.

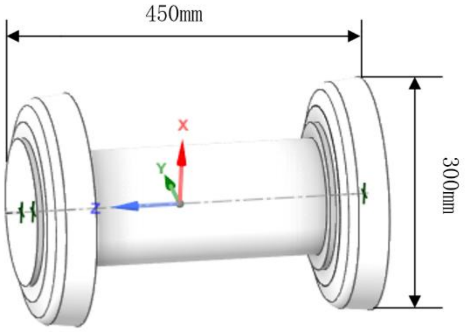


Fig. 1. Schematic diagram of the simplified pipeline robot

The maximum outer diameter of the pipe inspection robot is 300 millimeters, the inner diameter of the straight and bent pipe is 400 millimeters, the robot motion path always coincides with the axis of the pipe, ignoring the detection rod and mileage wheel, and retaining the more accurate geometry in the skin bowl structure at both ends of the inspection robot.

## 2.2 Reasonable Assumptions.

The fluid met is an incompressible Newtonian fluid, satisfying Newton's law of internal friction.

That the sliding friction between the support wheel and the pipe wall contact is neglected and the support wheel is always in contact with the pipe wall.

Disregard the effect of pressure and temperature changes on fluid viscosity and density.

No fluid leakage occurs inside the pipeline inspection robot.

The space occupied by the real fluid can be approximated as a continuous, gapless coverage that fills the entire pipe.

## 2.3 Fundamental Equations of Fluid Dynamics.

The motion of the pipeline inspection robot in the fluid satisfies the three conservation equations of fluid kinematics: energy conservation equation, mass conservation equation, and momentum conservation equation, and the mathematical expressions expressed in tensor form are shown below:

$$\frac{\partial \rho}{\partial t}+\frac{\partial \rho u_i}{\partial x_i}=0. \tag{1}$$

$$\frac{\partial\left(\rho u_i\right)}{\partial t}+\frac{\partial\left(\rho u_i u_j\right)}{\partial x_j}=-\frac{\partial p}{\partial x_j}+\frac{\partial \tau_{ij}}{\partial x_j}+\rho f_i. \tag{2}$$

$$\begin{aligned}\frac{\partial(\rho E)}{\partial t}+\frac{\partial\left(\rho E u_i\right)}{\partial x_i}=\rho \dot{q}+k \frac{\partial^2 T}{\partial x_i^2}-\frac{\partial\left(p u_i\right)}{\partial x_i} \\ +\frac{\partial\left(\tau_{ij} u_j\right)}{\partial x_i}+\rho f_i u_i\end{aligned}. \tag{3}$$

where $\rho$ is the gas density, is the time, $t$ is the time, $u$ is Air velocity, subscripts, c are subscripts; $p$ is the pressure, $\mu$ is the dynamic viscosity coefficient, $T$ is the temperature, $k$ is the thermal conductivity, $\delta_{ij}$ is the Kronecker coefficient, $f_i$ is the Volume force per unit mass of gas, $E$ is the Total energy per unit mass of gas, $E = e + 0.5u_i u_i$, $e$ is the Internal energy per unit mass of gas, $x$ is the right-angle coordinate component, $\dot{q}$ is the Heating rate per unit mass of gas, $\tau_{ij}$ is the Viscous stress tensor component.

$$\tau_{ij} = \mu\left(\frac{\partial u_i}{\partial x_j} + \frac{\partial u_j}{\partial x_i}\right) - \frac{2}{3}\mu\frac{\partial u_k}{\partial x_k}\delta_{ij} \tag{4}$$

## 3. Simulation Parameter Setting

### 3.1 Calculation Field Setting.

The entire computational domain is the pipe, in all parts of the pipe are filled with fluid, the left inlet of the straight pipe is 500mm according to the upper surface of the robot, the right outlet of the straight pipe is 1000 millimeters from the lower section of the robot, the inner diameter of the straight pipe and the bent pipe are 400 millimeters. the origin of the coordinate system is established on the pipe inspection robot, the positive and negative direction of the Z-axis is the direction of fluid movement, the XY plane is parallel to the cross section of the pipe.

### 3.2 Mesh.

A reasonable tetrahedral mesh division is used, while five boundary layers are set at the junction of the pipe wall and the fluid to reduce the influence of the pipe wall on the flow field and to ensure the reliability of the simulation results.

### 3.3 Solution Setting.

The inlet and outlet boundary conditions of velocity inlet and pressure outlet are used, the incoming flow velocity is 1m/s, the wall conditions are used on the surface of the pipe and the surface of the pipe detection robot, the fluid material is used to contrast water and kerosene, two kinds of liquids with different densities, the solid material of the pipe is selected as aluminum, the pipe type is straight and bent, due to the incompressibility of the liquid, the Mach number is lower than 0.3, according to the incompressibility of water and oil In the constant calculation, the SST k-w turbulence model is chosen, the SIMPLE algorithm is used for pressure-velocity coupling, the standard discrete format is used for pressure, and the second-order windward discrete format is used for momentum, turbulent kinetic energy, and turbulent dissipation rate. In the non-constant calculation, the steady-state flow field is used as the initial flow field, and the model is chosen as the realizable k-e turbulence model, and the coupled pressure-velocity algorithm is adopted as the coupled pressure-velocity model. The calculation time step is 0.005s, 20 iterations in each time step, and 1000 time steps. The parameter settings are basically the same for the straight pipe and the bent pipe.

## 4. Flow Field Characterization

### 4.1 Pressure Coefficient Distribution.

As shown in the Fig. 2 are the transient pressure distribution clouds (distribution in the ZX plane. The top and bottom are distinguished by the type of pipe, the left and right are distinguished by water and kerosene, the same below) of the pipeline inspection robot in a straight pipe filled with medium of water and medium of kerosene and in a bent pipe, respectively, it can be seen from the figure: the pressure coefficient distribution of the flow field has similarity.

In the straight pipe, the pressure coefficient of the flow field and the robot wall is greater when water is the medium, and the fluid has a greater pressure at the entrance, and the pressure gradually becomes smaller and then gradually increases after flowing through the side of the pipeline robot along the direction of motion, forming a positive and a negative pressure zone at both ends of the pipeline inspection robot, and forming a larger pressure difference at the entrance of both ends of the pipe to provide differential pressure driving force to the pipeline robot in two different media In the bend pipe, the pressure difference between the two ends of the pipe is greater when water is also used as the medium. The difference between the inlet and outlet pressure is 811.1602 Pa and 1011.454 Pa for the two different media.

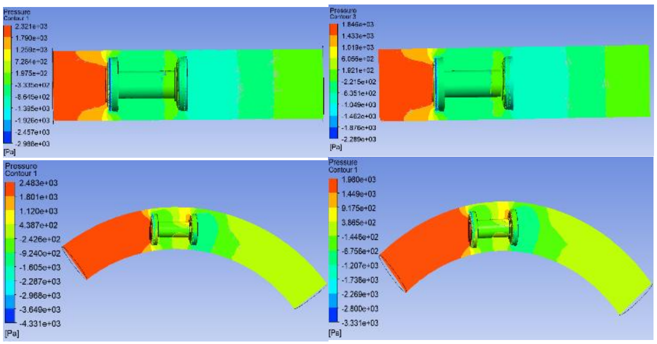

Fig. 2. Cloud of pressure coefficient distribution of pipeline robot under four working conditions

### 4.2 Transient Velocity Distribution.

As shown in the Fig. 3 and Fig, 4, the transient velocity distribution cloud and transient velocity vector diagram (distribution in the ZX plane) of the pipeline inspection robot under four working conditions, the transient velocity distribution law is roughly the same in the same pipe type, in the straight pipe, the fluid velocity increases sharply after flowing through the part of the maximum radius at the skin bowl of the pipeline inspection robot, and then gradually decreases along the direction of motion, and finally forms a longer, larger area in front of The velocity of the flow field around the robot is symmetrically distributed about the axis of the pipe, and the fluid disturbance characteristics are obvious. In the bend, two high-speed zones with gradually decreasing velocities are also formed on both sides of the pipe inspection robot, but the difference is that the flow field disturbance on the outside of the bend is more intense than that on the inside of the bend, forming a more chaotic disturbance area, which has a greater impact on the motion state of the pipe inspection robot.

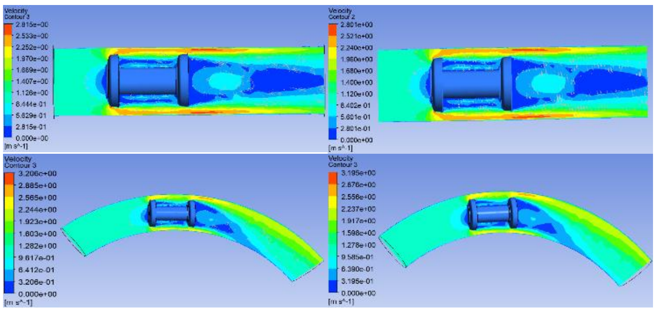

Fig. 3. Transient velocity cloud

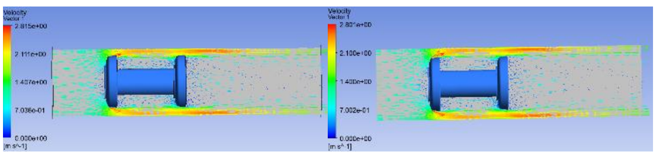

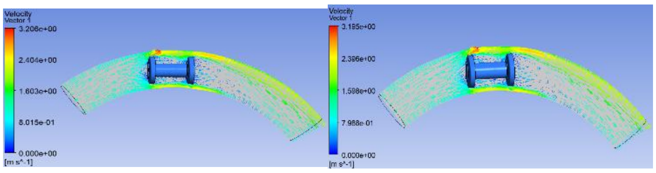

Fig. 4. Transient velocity vector cloud

### 4.3 Fluid Streamlines.

In order to see more clearly the characteristics of the flow field inside the pipe, as shown in the Fig. 5 for the four working conditions of the fluid trace map (distribution in the ZX plane), combined with the transient velocity cloud map for comparison, in the case of the same type of pipe, there is roughly the same distribution pattern. In the straight pipe, it can be found that the fluid flowing through the pipeline inspection robot at both ends of the deformation case, the flow is blocked, and the pipeline inspection robot on both sides of the fluid low velocity zone generated a speed difference and the formation of a certain degree of disturbance of the vortex, in the upper and lower sides with a certain symmetry of the vortex, in the direction of motion due to the rapid velocity changes around the flow field rolled up a certain degree of disturbance of the vortex structure, and forward dispersion, and With the distance becomes smaller and smaller. In the bend, three vortices of different shapes are formed, and the fluid disturbance on this side is more chaotic due to the greater change in airflow velocity on the outside of the pipe bend, and the motion speed of the pipe inspection robot is easily affected by the chaotic flow field around it, so more consideration is needed to solve the problem of unstable running speed when the robot crosses the bend.

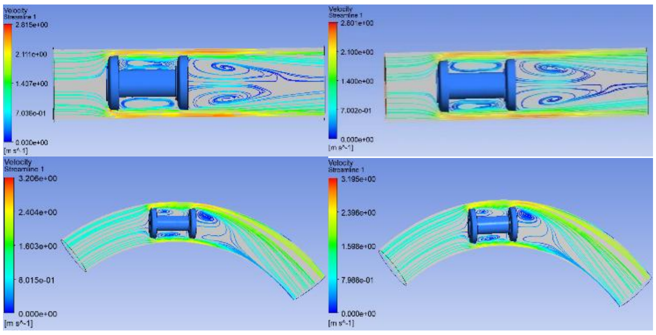

Fig. 5. streamline trace diagram

## 5. Conclusion

Compared with other motor-driven and hybrid energy-driven pipeline inspection robots, they have higher speed stability in the pipeline and can make effective control of their speed after entering the pipeline, while fluid pressure differential drive is more difficult to achieve different speed control directly by controlling the differential pressure at the two ends of the pipeline entrance and exit, which is less controllable, but can avoid the situation that the pipeline robot stops running without power in the pipeline. The speed control is less controllable. In different media, the pressure difference between the two ends of the pipeline inspection robot has a relatively obvious difference, and the flow field pressure coefficient distribution and velocity distribution around the similarity, in a denser, less viscous medium, the flow field pressure around the robot becomes larger, and the pressure difference between the inlet and outlet on both sides of the pipeline increases, so the robot can obtain a greater differential pressure driving force without changing itself, and can complete the pipeline inspection operation more quickly at the same pipeline inlet flow rate. The robot is able to complete the pipeline inspection operation faster with the same inlet flow rate. Under the same medium, straight pipes and bends have different flow field characteristics. The pressure difference between the front and rear ends of straight pipes is easy to control, and the flow field characteristics are simpler, while due to the special characteristics of bends, the pressure difference between the two ends of the detection robot is asymmetric, and the flow field around it is more disturbed. Reasonable design of the pipeline inspection robot shape, reduce the impact of flow field disturbance on the operating speed, can make the robot have a better operating effect.

## Acknowledgement

This paper was supported by National Natural Science Foundation of China (Grant number 51975024).

## References

[1] Shi Yan, Mu Zhenxin, Cai Maolin, et al. Advances in motion control of gas pipeline detection robot. Science China-Technological Sciences, 2019,63(5):877-878.

[2] Xingyuan Miao, Hong Zhao, Boxuan Gao, Yinghan Ma, Yanguang Hou, Fulin Song, Motion analysis and control of the pipeline robot passing through girth weld and inclination in natural gas pipeline. Journal of Natural Gas Science and Engineering, 2022, 104.

[3] Tao Zheng et al. Design of a robot for inspecting the multishape pipeline systems. IEEE-ASME Transactions on Mechatronics, 2022, 27(6):4608-4618.

[4] Shi Yan, Hao Liming, Cai Maolin, et al. High-precision diameter detector and three-dimensional reconstruction method for oil and gas pipelines. Journal of Petroleum Science and Engineering, 2018, 165:842-849.

[5] Liu Xiaomin, Song Maozheng, Fang Yuhui, et al. Worm-inspired soft robots enable Adaptable Pipeline and Tunnel Inspection. Advanced Intelligent Systems, 2021, 4(1).

[6] Yan Hongwei, Wang Lu, Li Pengcheng, et al. Research on passing ability and climbing performance of pipeline plugging robots in curved pipelines. IEEE Access, 2020, 8:173666-173680.

[7] Mingze Gao, Min Huang, Kai Tang, Xuqiang Lang, Jiaming Gao. Design, analysis, and control of a multilink magnetic wheeled pipeline robot. IEEE Access, 2022, 10:67168-67180.

[8] Tang Chao, Du Boyun, Jiang Songwen, et al. A pipeline inspection robot for navigating tubular environments in the sub-centimeter scale. Science Robotics, 2022, 7(66).

[9] Zhang Hang, Dong Jinhui, Cui Can, et al. Stress and strain analysis of spherical sealing cups of fluid-driven pipeline robot in dented oil and gas pipeline. Engineering Failure Analysis, 2019,108.

[10] Rashid M Z A , Yakub M F M , Salim S A Z B S ,et al. Modeling of the in-pipe inspection robot: A comprehensive review. Ocean Engineering, 2020, 203

[11] Lei Xu, Yunfu Wang, Lin Mo, Yongfan Tang, Feng Wang, Changjun Li, The research progress and prospect of data mining methods on corrosion prediction of oil and gas pipelines. Engineering Failure Analysis, 2023, 144.